Semicond. Sci. Technol. **10** (1995) 627–633. Printed in the UK

Evaluation of the minority carrier diffusion length by means of electron beam induced current and Monte Carlo simulation in AlGaAs and GaAs p–i–n solar cells

Enrique Grünbaum†‡§, Eli Napchan||, Zahava Barkay¶, Keith Barnham††, Jenny Nelson††, C Tom Foxon‡‡, John S Roberts§§ and David B Holt||

† Interdisciplinary Research Centre for Semiconductor Materials, Imperial College of Science, Technology and Medicine, London SW7 2BZ, UK
‡ Department of Physical Electronics, Faculty of Engineering, Tel-Aviv University, Ramat-Aviv 69978, Israel
|| Department of Materials, Imperial College of Science, Technology and Medicine, London SW7 2BZ, UK
¶ School of Physics and Astronomy, Tel-Aviv University, Ramat-Aviv 69978, Israel
†† Blackett Laboratory, Imperial College of Science, Technology and Medicine, London SW7 2BZ, UK
‡‡ Physics Department, University of Nottingham, Nottingham NG7 2RD, UK
§§ SERC III–V Facility, University of Sheffield, Sheffield S1 3JD, UK

Received 7 September 1994, accepted for publication 19 December 1994

Abstract. A new method of determining the minority carrier diffusion length in multilayer solar cells is described. Electron beam-induced current (EBIC) gain measurements, performed in a scanning electron microscope in the planar sample configuration, are compared with values obtained by calculations using a Monte Carlo simulation program of electron trajectories. Values for diffusion lengths obtained by this method from five AlGaAs and GaAs p–i–n and p–n solar cells are compared with values given in the literature.

1. Introduction

The quantum well solar cell, which is a novel approach to higher efficiency, has been the subject of intensive research [1,2]. It is basically a p–i–n structure made from a semiconductor, such as $Al_xGa_{1-x}As$ or GaAs, containing a system of quantum wells of lower-bandgap material (GaAs or InGaAs respectively) within the undoped region. For the modelling of the current and voltage characteristics of these cells, the values of the minority carrier diffusion lengths L_n and L_p of the electron and holes in the p and n regions respectively, and of the width and location of the depletion region w_d are required.

The electron beam-induced current (EBIC) method is a very powerful technique for the characterization of semiconductors [3]. There are two sample configurations for performing the measurements: the planar one, in which the primary electron beam is incident at a fixed point (or area) perpendicular to the cell surface and to the p–i–n junction; and the cross-sectional one, in which the primary electron beam is incident parallel to the p–n or p–i–n junction and scanned in a line perpendicular to it. For the solar cells used in this study, the former configuration is particularly suitable as the p-region, which contributes substantially to the photocurrent, is thin (0.15–0.5 μm).

A new method is presented here for determining the electrical characteristics, mentioned above, in multilayer structures by comparing experimental EBIC gain measurements with the gain values obtained from a Monte Carlo simulation program. It can be applied not only to the p–i–n and p–n multilayer structures used in solar cells, presented here, but in general to those used in other optoelectronic devices (e.g. lasers) or in electronic devices (e.g. high electron mobility transistors). In this

§ Permanent address: Department of Physical Electronics, Faculty of Engineering, Tel-Aviv University, Ramat-Aviv 69978, Israel.

0268-1242/95/050627+07$19.50 © 1995 IOP Publishing Ltd

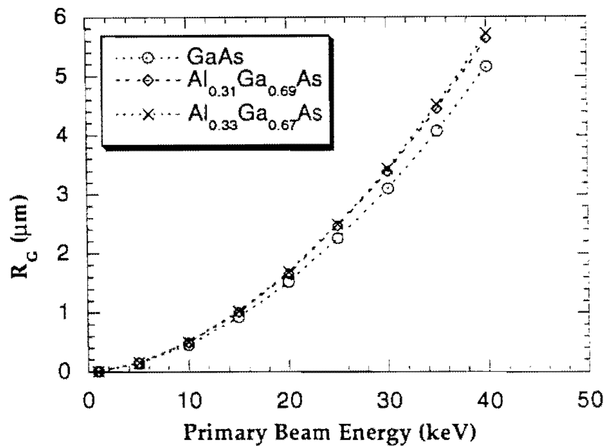

Figure 1. Grün electron penetration range R_G as a function of primary electron beam energy E_b for $Al_xGa_{1-x}As$ and GaAs, calculated using equation (2).

method the gain (G) is determined experimentally for various primary electron energies (E_b):

$$G = I/I_b \qquad (1)$$

where I is the EBIC, or short-circuit current, and I_b is the primary beam current. The change in E_b gives rise to different values of the electron penetration range, which can be calculated for a single material specimen by Grün's formula [3] (called the Grün range or R_G)

$$R_G = (0.0428/\rho)E_b^{1.75}\ (\mu\text{m}) \qquad (2)$$

where ρ is the material density (g cm^{-3}) and E_b is expressed in keV (figure 1). This relationship demonstrates that the centre of the interaction volume of the electrons ($\approx 0.41R_G$) is located at different depths of the multilayer system for different E_b; the values of L_n and L_p can thus be determined separately by changing E_b. For the determination of these values, the experimentally obtained gain is compared with that obtained by theoretical calculations. In the model adopted, the incident electrons lose their energy gradually along their trajectories, which is determined both by elastic and inelastic scattering. A large number of electron–hole pairs Δn_g is created, whose volume density is

$$\Delta n_g = \Delta E/e_i \qquad (3)$$

where ΔE is the (calculated) electron energy per unit volume deposited at depth z from the cell surface and e_i is the electron–hole pair formation (or 'ionization') energy, which is given in terms of the bandgap E_g by either of the two following formulae:

$$e_i = 2.1E_g + 1.3\ (\text{eV}) \qquad (4a)$$

which is the one used here, or

$$e_i = 3E_g\ (\text{eV}) \qquad (4b)$$

where E_g is the energy bandgap.

The calculations are performed by a Monte Carlo simulation program of the electron trajectories, as developed by one of us [4–8] for a multilayer system (up to 10 layers), such as used in solar cells. From the simulation, the energy dissipation ΔE and energy-depth dose dE/dz are obtained as a function of depth z. The fraction of the primary beam energy lost by backscattered electrons has been taken into account during the tracking of each primary electron trajectory. The EBIC is the result of the sum of all those generated carriers which are able to reach the depletion region without suffering recombination. They are then swept by the electric field existing in the depletion region, together with those generated in this region, to the electrodes. The fraction of the carriers reaching the depletion region is given by the factor $\exp(-z_d/L)$, where z_d is the distance from the point of generation to the corresponding edge of the depletion region and L is the minority carrier diffusion length. The collection efficiency of the depletion region is assumed to be 100%. Attached to the simulation program is a calculation programme of EBIC gain values, using proposed values for the electrical parameters L_n, L_p and the location of the depletion region of width w_d. These calculated gain values are then compared with the experimentally obtained ones. Surface recombination has not been taken into account in this program.

2. Experimental set-up and results

The EBIC measurements were performed in JEOL 840-A and Philips SEM 505 scanning electron microscopes. The header on which the solar cell specimens were mounted was directly attached by its pins to the contacts of a ceramic holder located on the microscope table. No prior specimen preparation was needed. To reduce specimen carbon contamination from the residual hydrocarbons in the microscope and heating effects, the electron beam was scanned over an area of 10–100 µm in

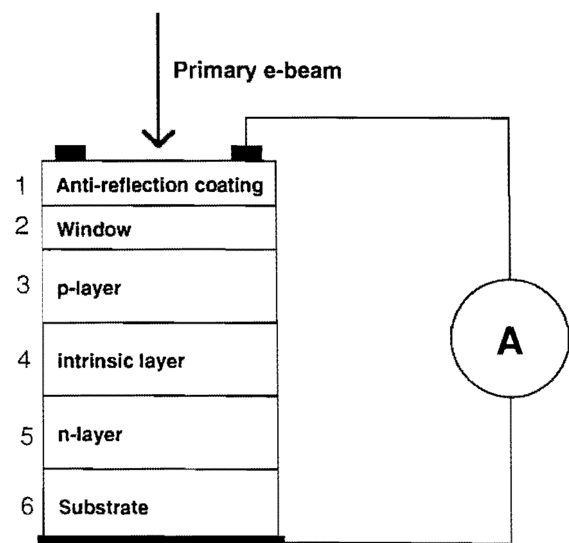

Figure 2. Multilayer arrangement of solar cell and experimental set-up.

Table 1. Layer arrangement in control solar cells.

Layers		$Al_{33}Ga_{67}As$ p–i–n (G947)			$Al_{33}Ga_{67}As$ p–n (QT468c)			$Al_{31}Ga_{69}As$ p–i–n (QT231+AR)			GaAs p–i–n and GaAs p–i(5QW)–n (QT419b+AR and QT422a+AR, resp.)		
No	Function	x (%)	Width (μm)	n (cm^{-3})	x (%)	Width (μm)	n (cm^{-3})	x (%)	Width (μm)	n (cm^{-3})	x (%)	Width (μm)	n (cm^{-3})
1	Cap or AR	0	0.017	$p = 2 \times 10^{18}$	0	0.04	$p = 2 \times 10^{18}$	SN	0.18		SN	0.075	
2	Window				80	0.02	$p = 2 \times 10^{18}$	80	0.045	$p = 2 \times 10^{18}$	80	0.043	$p = 1 \times 10^{18}$
3	p	33	0.15	$p = 1.3 \times 10^{18}$	33	0.15	$p = 1.3 \times 10^{18}$	31	0.50	$p = 2 \times 10^{18}$	0	0.50	$p = 2 \times 10^{18}$
4	i	33	0.51	$p = 5 \times 10^{14}$	—	0	—	31	0.80	$p = 1 \times 10^{15}$	0	0.32	$p = 1 \times 10^{14}$
5	n	33	0.46	$p = 1.3 \times 10^{18}$	33	0.60	$n = 6 \times 10^{17}$	31	0.50	$n = 6 \times 10^{17}$	0	2.00	$n = 1.3 \times 10^{17}$
6	Buffer	0	0.51	$n = 2 \times 10^{18}$							0	0.30	$n = 2 \times 10^{18}$
7	Substrate	0		n^+	0		n^+	0		n^+	0		n^+

Abbreviations: AR = antireflection; x = composition; n = carrier concentration; SN = S_3N_4; for 5QW see text.

Table 2. Data for materials used for simulation.

Compound	Abbreviation	Z	A (g mole^{-1})	ρ (g cm^{-3})	E_g (eV)	e_i: $2.1E_g + 1.3$ (eV)	e_i: $3E_g$ (eV)
Si_3N_4	SN	10.00	20.00	3.10		15.9	
$Al_{0.80}Ga_{0.20}As$	AE	24.8	55.2	4.08	2.43	6.3	7.3
$Al_{0.33}Ga_{0.67}As$	AU	29.0	65.3	4.79	1.84	5.2	5.3
$Al_{0.31}Ga_{0.69}As$	AT	29.2	65.7	4.86	1.81	5.1	5.4
GaAs	AG	32.0	72.3	5.32	1.42	4.3	4.3

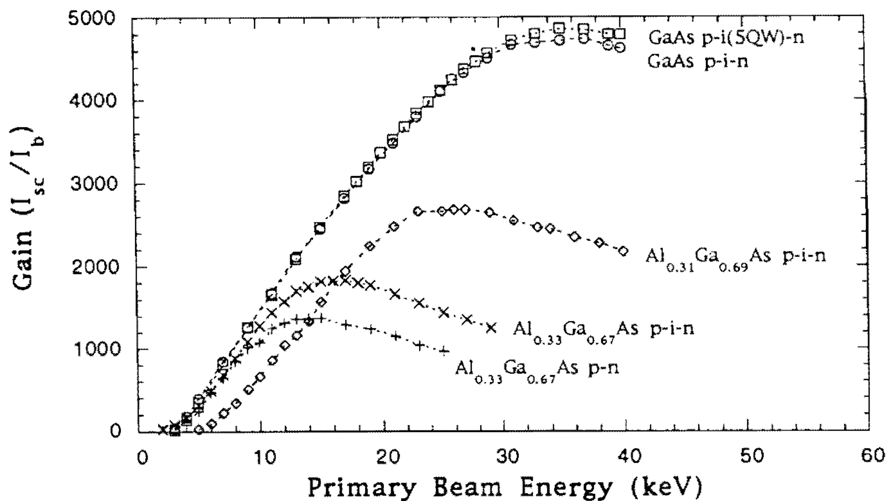

Figure 3. EBIC gain measured as a function of beam energy E_b for the five samples described in table 1.

extension during the measurement. The primary electron beam was measured either by a pneumatically retractable Faraday cage mounted in the microscope column above the specimen or by a Faraday cage mounted on the table close to the specimen before and after each EBIC measurement. It was adjusted to about 1 nA before starting the EBIC measurements. A variable-gain current amplifier (Matelect ISM-5 with an ICA-1 head amplifier, or Keithley 427) was used for measuring the EBIC and beam current.

The multilayer arrangement of the solar cells and the experimental set-up are shown in figure 2. Four different types of $Al_xGa_{1-x}As$ and GaAs p–i–n and p–n solar cells have been analysed; their composition (x), width (w) and dopant concentration (n) are specified in table 1. The p–i–n solar cells were grown under the same conditions and had the same layer arrangement as the solar cells containing quantum wells in the i region,

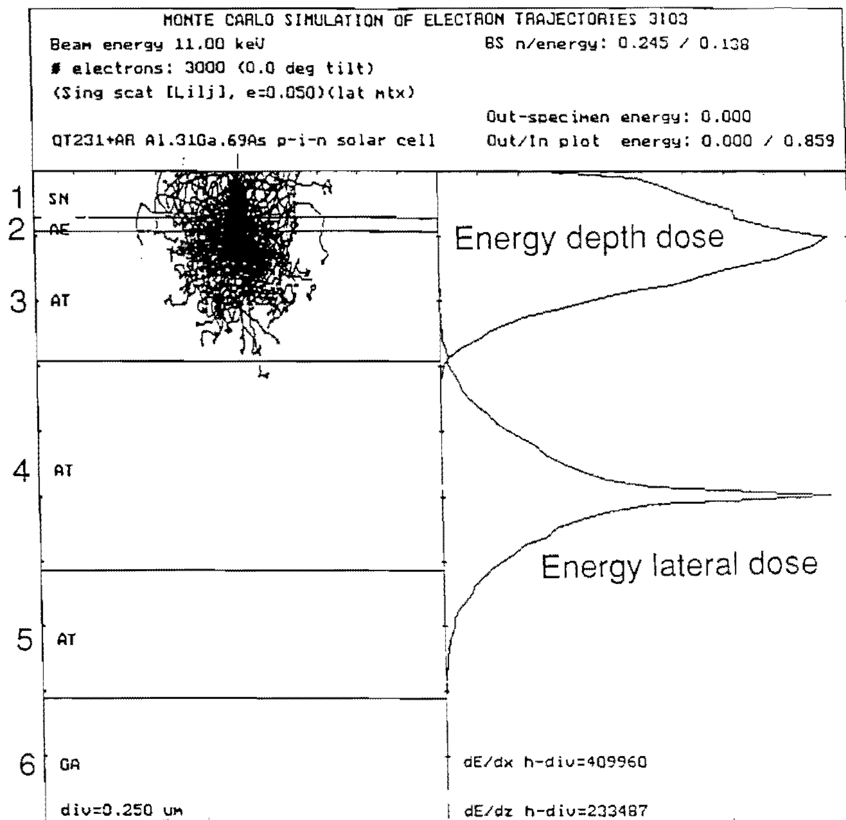

Figure 4. Monte Carlo simulation of electron trajectories in the $Al_{0.31}Ga_{0.69}As$ p–i–n solar cell QT231 for three different values of primary beam energy: (*a*) 11 keV, (*b*) 17 keV and (*c*) 21 keV. In the left panels are shown the electron trajectories as simulated for the first 200 electrons; the different layers of the multilayer system are drawn to scale according to the separations specified in table 1. The centre panels show the energy–depth dose dE/dz as a function of z and the percentage (E) of the primary energy deposited in each layer ((*a*) also shows the lateral energy dose dE/dx as a function of x). The right-hand panels give the simulated gain values as follows: in (*b*) as a function of L_n with $w_d = w_i$; and in (*c*) as a function of L_p, with L_n fixed and $w_d = w_i$.

but their i region was homogeneous. A fifth solar cell containing multiquantum wells (QT422a+AR) has also been measured; it had the same layer arrangement as the GaAs p–i–n cell (QT419b+AR), except that its i-region contained five quantum wells of $In_{0.2}Ga_{0.8}As$, each 80 Å wide, separated by 500 Å GaAs barriers, all undoped, and a 300 Å wide GaAs buffer layer. Sample G947 was grown by MBE (at the Philips Research Laboratories) and the other four samples by MOVPE (at the University of Sheffield). Further details are given in [2] and the references therein.

EBIC gain has been measured as a function of beam energy at zero bias (figure 3). In each of the curves, a nearly linear increase of G up to a maximum value is observed, followed by a slower decrease with E_b. This is explained by the increase with E_b of the total number of carriers generated per incident beam electron ($n_g = E_b/e_i$, approximately), whilst at the same time the centre of the energy deposition region moves deeper into the material (equation (2) and figure 1); when it moves beyond the depletion region into the n-region, the collection efficiency is reduced and hence G gradually approaches a maximum and then decreases slowly. In the depletion region (which approximately coincides with the i-region or with the p–n junction, for the p–i–n and p–n cells respectively), the carriers move by drift in the electric field due to the built-in potential, as no bias is applied; the collection efficiency in that region is very high (assumed here to be 100%).

3. Monte Carlo simulation strategy and results

The MC-SET computer program for Monte Carlo simulation of electron trajectories and energy deposition, devised by one of us [6], was used for the calculation of the EBIC gain for each of the four samples and for the various beam energies used in the experiments. The single-scattering model was employed for better accuracy in the calculation of the relatively thin layers of the solar cells, with 3000 incident electrons per simulation. The data of the layer arrangement and of the atomic number Z and atomic mass A (calculated from the atomic mass weighted average of the values of the compound elements) and the material density ρ of the various materials introduced into the simulation program are listed in tables 1 and 2, respectively.

The simulation for each sample and energy is divided into two stages. First an energy file, which contains the energy deposited as a function of depth, is created.

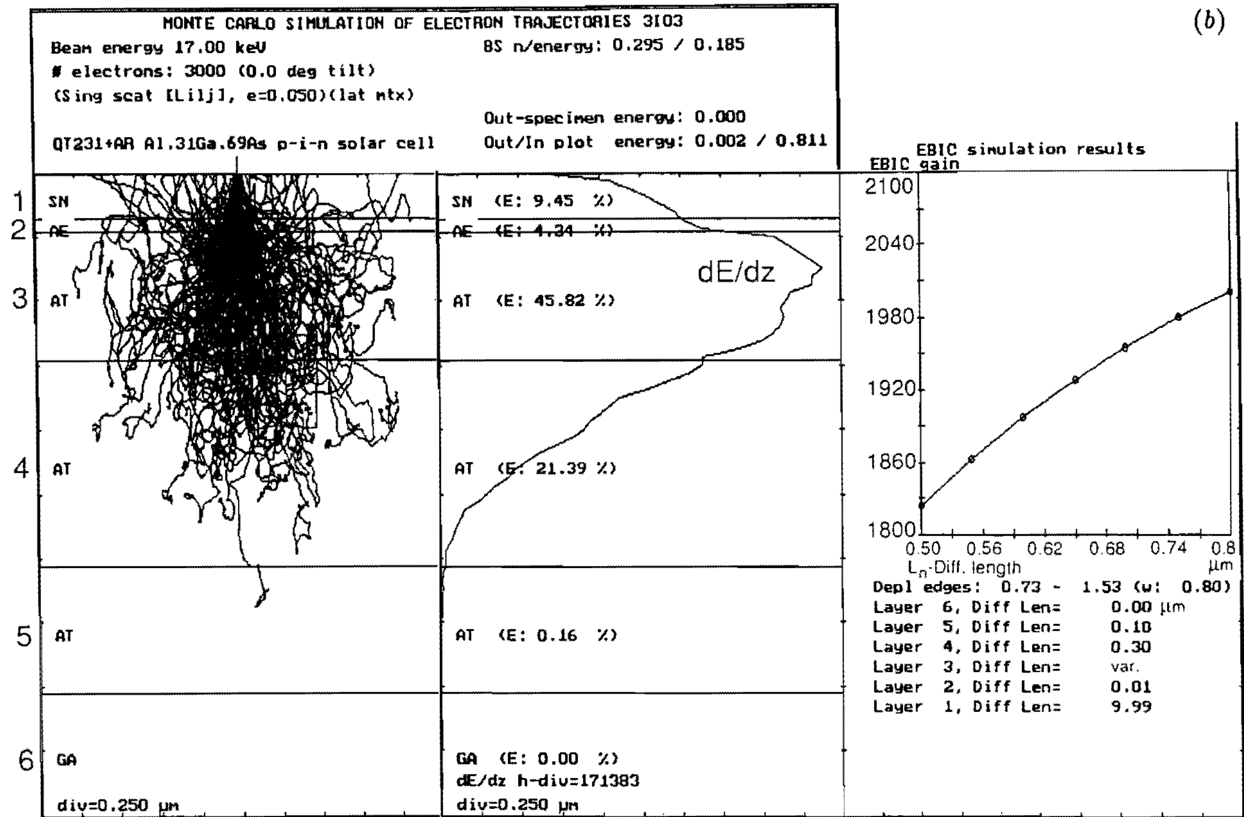
(b)
MONTE CARLO SIMULATION OF ELECTRON TRAJECTORIES 3103
Beam energy 17.00 keV
BS n/energy: 0.295 / 0.185
electrons: 3000 (0.0 deg tilt)
(Sing scat [Lilj], e=0.050)(lat mtx)
Out-specimen energy: 0.000
QT231+AR Al.31Ga.69As p-i-n solar cell
Out/In plot energy: 0.002 / 0.811
SN (E: 9.45 %)
AE (E: 4.34 %)
AT (E: 45.82 %)
AT (E: 21.39 %)
AT (E: 0.16 %)
GA (E: 0.00 %)
dE/dz
dE/dz h-div=171383
div=0.250 µm
EBIC simulation results
EBIC gain
Ln-Diff. length µm
Depl edges: 0.73 - 1.53 (w: 0.80)
Layer 6, Diff Len= 0.00 µm
Layer 5, Diff Len= 0.10
Layer 4, Diff Len= 0.30
Layer 3, Diff Len= var.
Layer 2, Diff Len= 0.01
Layer 1, Diff Len= 9.99

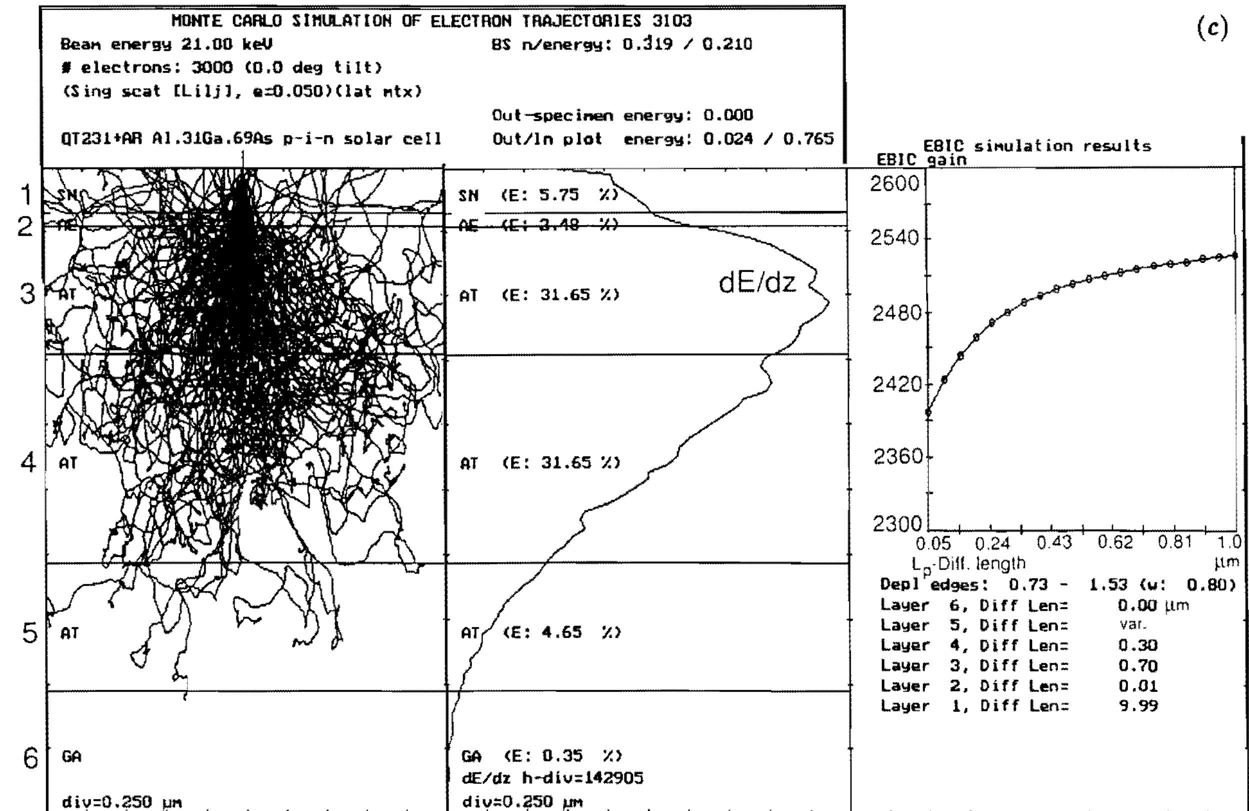
(c)
MONTE CARLO SIMULATION OF ELECTRON TRAJECTORIES 3103
Beam energy 21.00 keV
BS n/energy: 0.319 / 0.210
electrons: 3000 (0.0 deg tilt)
(Sing scat [Lilj], e=0.050)(lat mtx)
Out-specimen energy: 0.000
QT231+AR Al.31Ga.69As p-i-n solar cell
Out/In plot energy: 0.024 / 0.765
SN (E: 5.75 %)
AE (E: 3.48 %)
AT (E: 31.65 %)
AT (E: 31.65 %)
AT (E: 4.65 %)
GA (E: 0.35 %)
dE/dz
dE/dz h-div=142905
div=0.250 µm
EBIC simulation results
EBIC gain
Lp-Diff. length µm
Depl edges: 0.73 - 1.53 (w: 0.80)
Layer 6, Diff Len= 0.00 µm
Layer 5, Diff Len= var.
Layer 4, Diff Len= 0.30
Layer 3, Diff Len= 0.70
Layer 2, Diff Len= 0.01
Layer 1, Diff Len= 9.99

Three typical graphs obtained from these files are shown in figure 4 (left and centre panels) for the $Al_{0.31}Gas_{0.69}As$ p–i–n solar cell QT 231 with beam energies of 11, 17 and 21 keV. These graphs were chosen for energies for which the electron range is expected to reach the lower edge of the p, i and n regions respectively (compare with the values of figure 1). Figure 4(c) also corresponds to the beam energy which produces a gain close to the maximum for that particular cell.

In the second stage, an extensive study of the gain as a function of the electrical parameters mentioned above is made separately for simulation runs obtained at different E_b values, using the calculation scheme contained in the same MC-SET program. A comparison of the simulated G values with those obtained experimentally allows the choice of the best values for L_n and L_p. A convenient procedure for the p–i–n cells is to start the simulations with an E_b for which the penetration range is up to the edge of the i-region; L_n is chosen as the variable parameter and the depletion width (w_d) is assumed to be equal to the width of the intrinsic region (w_i) (figure 4(b), right panel). Then a higher value of E_b is taken, for which the penetration depth is up to the edge of the n-region, and, using the value of L_n found in the previous step, L_p is determined (figure 4(c), right panel). Iterations with other values of E_b could give improved values of these parameters, including those for which the electron beam penetrates the substrate, by assuming an adequate value for L_p of the substrate. The graphs (figure 4, right panels) also allow an estimation of the errors involved in the choice of the parameters.

In the case of the p–n cell, the simulations should be started with a value of E_b corresponding to a penetration range up to the edge of the p-region, taking L_n as variable and w_{dp} and w_{dn} (the widths of the depletion region within the p and n region respectively) as the calculated values from the known dopant concentrations and $w_d = w_{dp} + w_{dn}$. Then one proceeds with a higher value of E_b for which the penetration depth is up to the edge of the n-region for the evaluation of L_p using the value of L_n previously determined.

Figures 5 and 6 show the simulated gain values, giving the best fit with the experimental ones, for the p–i–n cell QT 231 and the p–n cell QT468c respectively. The relative gain values obtained by calculation are also plotted, allowing a better appreciation of the fit. The values of the parameters chosen for the best fit simulations of the five solar cells studied are summarized in table 3. The values of L_n and L_p are compared with those obtained from the formula given by Hamaker [9] for $Al_xGa_{1-x}As$, as a function of x and various dopant concentrations.

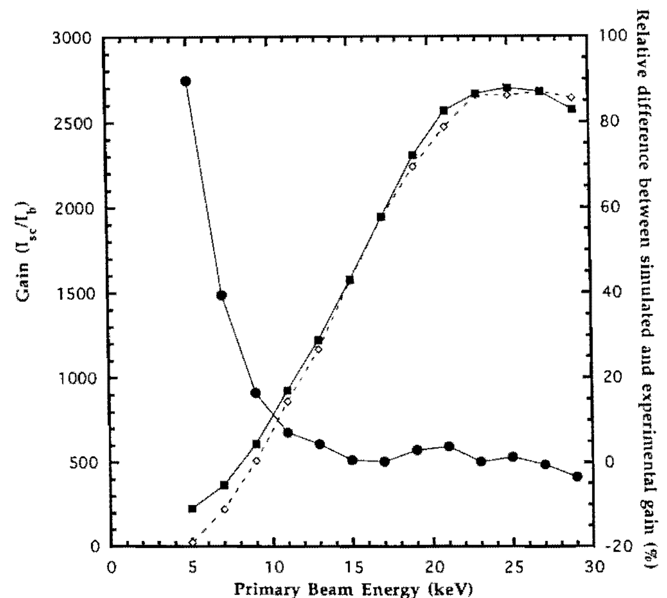

Figure 5. Gain as a function of E_b for the same sample as that of figure 4: ◊, experimentally determined values, taken from figure 3; ■, values obtained by simulation with the parameters which give the best fit (L_n = 0.73 μm, L_p = 0.10 μm, L_p for the substrate=0 μm and $w_d = w_i$ = 0.80 μm). On the same graph, the relative difference in gain (●) is expressed as [100× (simulated value-experimental value)/simulated value] as a function of E_b.

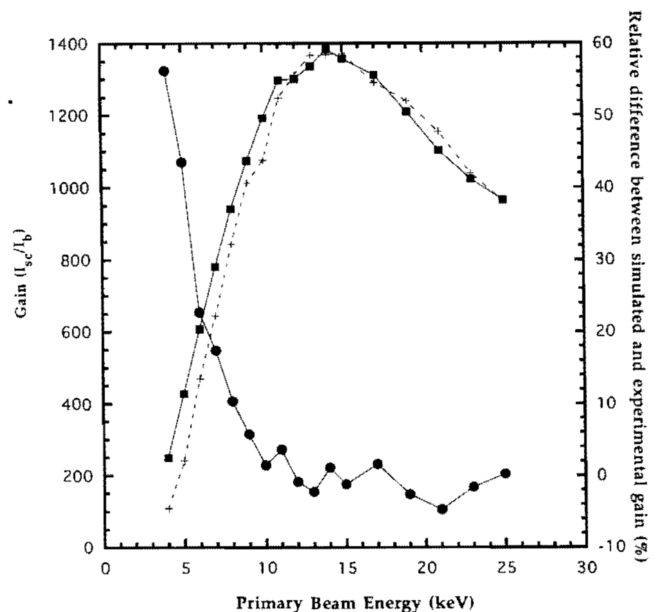

Figure 6. Gain as a function of E_b for the $Al_{0.33}Ga_{0.67}As$ p–n solar cell QT468c: +, experimentally determined values, taken from figure 3; ■, values obtained by simulation with the parameters which give the best fit (L_n = 0.50 μm; L_p = 0.32 μm; w_{dp} = 0.04 μm; w_{dn} = 0.06 μm). The relative difference in gain (●) was calculated as for figure 5.

4. Discussion

The choice of the planar sample configuration for performing the measurements has the advantage of avoiding specimen preparation. In the cross-sectional configuration obtained by cleaving or cutting the specimen, a new surface is created. This introduces surface recombination effects, unknown backscattering and a non-uniform EBIC response.

Front surface recombination has been neglected in

Table 3. Monte Carlo simulation results.

	$Al_{0.33}Ga_{0.67}As$ p–i–n		$Al_{0.33}Ga_{0.67}As$ p–n		$Al_{0.31}Ga_{0.69}As$ p–i–n		GaAs p–i–n	
	Sim.G947	[9]	Sim.QT468c	[9]	Sim.QT231	[9]	Sim.QT419b	[9]
L_n (μm)	0.20	0.10	0.50	0.15	0.73	0.15	2.5	4
L_p (μm)	0.03	0.04	0.32	0.05	0.10	0.06	2.5	2.5
w_{dp} (μm)	0[a]		0.04[a]		0[a]		0[a]	
w_{dn} (μm)	0[a]		0.06[a]		0[a]		0[a]	
w_d (μm)	0.51[b]		0.10[a]		0.80[b]		0.32[b]	

[a] Values obtained by calculation.
[b] These values are equal to w_i as given in table 1.

the simulation model. This does not pose a serious problem in the present samples where a front window reduces considerably the surface recombination. Also, the possible effect of the contamination of the sample surface by deposited carbon, due to the decomposition by the electron beam of the residual hydrocarbons in the scanning electron microscope, has not been taken into account. The influence of these surface effects is expected to be reduced at the higher beam energies, with the interaction volume extending further into the specimen. In fact, as can be seen in figures 5 and 6, the values of the simulated gain are much larger than those of the experimental one for the very low beam energies and this relative difference gradually decreases until it vanishes. This occurs in figures 5 and 6 at E_b values of 17 and 12 keV, energies for which the primary beam just reaches the edge of the i region in sample QT231 and the n region in sample QT468c respectively. We chose these energies for exact fitting of the gain values by appropriate selection of L_n, in accordance with the procedure given in the previous section.

For the p–i–n cells, we have taken the width of their depletion region equal to that of the intrinsic region, because no significant penetration of the depletion region into the p and n regions is expected from a calculation based on the high dopant concentration and a much reduced field in these regions (for sample QT231, x_{dp} = 0.0005 μm and x_{dn} = 0.003 μm at zero bias). It can be shown from the simulations (figure 4(*c*)) that a small extension of the depletion region would have a considerable effect on the simulated gain, and a different value for L_n will have to be selected for a good fit with the experimental gain. It should be noted that, in general, w_d cannot be obtained independently of L_n by the fitting procedure outlined above, as the shape of the simulated gain curve does not depend on its value.

The accuracy of the determination of the electrical parameters L_n, L_p, w_{dp} and w_{dn} depends on that of the thickness of the layers given in table 1. These are the values given in the growth program; although they have been checked by modelling their spectral response as solar cells and comparing them with the experimental values [10], the actual values could be determined, for example by secondary-ion mass spectrometry or cross-section transmission electron microscopy of the samples.

The diffusion lengths determined by the present method, based on EBIC measurements for $Al_xGa_{1-x}As$, are larger than those quoted by Hamaker [9], which he states are based on measured values of the appropriate material parameters of $Al_xGa_{1-x}As$ (details are not given in his paper). This discrepancy can be explained by the improved growth process now used, leading to the reduction of impurities and defects which act as recombination centres, and hence to larger diffusion lengths.

5. Conclusions

A new method for obtaining L_n and L_p in multilayer devices has been developed which can be directly used on devices and is non-destructive. In general, the results are consistent with expectation. However, they indicate that the $Al_xGa_{1-x}As$ minority diffusion lengths are longer than those obtained from the formulae given in [9].

Acknowledgments

We wish to thank Professor Bruce Joyce and Professor Gareth Parry for making available the facilities of the Interdisciplinary Research Centre for Semiconductor Materials and for their encouragement. EG wishes to thank them also for their hospitality during his sabbatical year.

References

[1] Barnham K W J and Duggan G 1990 *J. Appl. Phys.* **67** 3490
[2] Barnham K W J, Barnes J, Haarpaintner G, Nelson J, Paxman M, Foxon T and Roberts J 1993 *Mater. Res. Soc. Bull.* **18** 51
[3] Holt D B 1989 *SEM Microcharacterization of Semiconductors* ed D B Holt and D C Joy (New York: Academic) pp 241–338
[4] Napchan E and Holt D B 1987 *Microscopy of Semiconducting Materials 1987 (Inst. Phys. Conf. Ser. 87)* ed A G Cullis and P Augustus (Bristol: Institute of Physics) pp 733–8
[5] Napchan E 1989 *Rev. Phys. Appl.* **4** C6-15
[6] Napchan E 1992 *Microscopy Anal.* (November) 9
[7] Farhang H, Napchan E and Blott B H 1993 *J. Phys. D: Appl. Phys.* **26** 2266
[8] Holt D B and Napchan E 1994 *Scanning* **16** 78
[9] Hamaker H C 1985 *J. Appl. Phys.* **58** 2344
[10] Paxman M, Nelson J, Braun B, Connolly J and Barnham K W J 1993 *J. Appl. Phys.* **74** 614